Journal of Groundwater Science and Engineering
ISSN 2305-7068
Indexed by ESCI CABI CSA
Scopus GeoRef AJ CNKI

Mechanism of seepage heat transfer in thermal reservoirs of high temperature metamorphic rocks in the Yanggao-Tianzhen basin

Mei-hua Wei, Yan-guang Liu, Xin Wang, Gao-jing Ren, Chao Xu, Jing-wen Liu, Ying-nan Zhang, Xu-cai Zhang

Citation:
Wei MH, Liu YG, Wang X, Ren GJ, Xu C, Liu J-W, Zhang Y-N, Zhang X-C. 2026. Mechanism of seepage heat transfer in thermal reservoirs of high temperature metamorphic rocks in the Yanggao-Tianzhen basin. Journal of Groundwater Science and Engineering, 14(3): 323-341.

View online: https://doi.org/10.26599/JGSE.2026.9280085

Articles you may be interested in

Research progress on temperature field evolution of hot reservoirs under low-temperature tailwater reinjection
Journal of Groundwater Science and Engineering. 2024, 12(2): 205-222 https://doi.org/10.26599/JGSE.2024.9280016

Simulation of thermal breakthrough factors affecting carbonate geothermal-to-well systems
Journal of Groundwater Science and Engineering. 2023, 11(4): 379-390 https://doi.org/10.26599/JGSE.2023.9280030

Characterization of rock thermophysical properties and factors affecting thermal conductivity–A case study of Datong Basin, China
Journal of Groundwater Science and Engineering. 2024, 12(1): 4-15 https://doi.org/10.26599/JGSE.2024.9280002

Quantitative study on vertical distribution of heat flow in Niutuozhen geothermal field, Xiong'an New Area—Evidence from heat flow determination in the Archean of D01 well
Journal of Groundwater Science and Engineering. 2025, 13(1): 22-33 https://doi.org/10.26599/JGSE.2025.9280036

Development status and prospect of underground thermal energy storage technology
Journal of Groundwater Science and Engineering. 2024, 12(1): 92-108 https://doi.org/10.26599/JGSE.2024.9280008

Progress and prospect of mid-deep geothermal reinjection technology
Journal of Groundwater Science and Engineering. 2024, 12(3): 321-338 https://doi.org/10.26599/JGSE.2024.9280024

Journal homepage: http://gwse.iheg.org.cn

Research Article

Mechanism of seepage heat transfer in thermal reservoirs of high temperature metamorphic rocks in the Yanggao-Tianzhen basin

Mei-hua Wei[1,2], Yan-guang Liu[3,4,5*], Xin Wang[4,5*], Gao-jing Ren[1,2], Chao Xu[1,2], Jing-wen Liu[1,2], Ying-nan Zhang[4,5], Xu-cai Zhang[3]

[1] *Shanxi Geological Engineering Exploration Institute Co., Ltd.*, *Taiyuan* 030024, *China*.
[2] *Shanxi Key Laboratory for Exploration and Exploitation of Geothermal Resources*, *Taiyuan* 030024, *China*.
[3] *Institute of Hydrogeology and Environmental Geology*, *Chinese Academy of Geological Sciences*, *Xiamen* 361021, *Fujian Province*, *China*.
[4] *Technology Innovation Center of Geothermal & Hot Dry Rock Exploration and Development*, *Ministry of Natural Resources Shijiazhuang* 050061,*China*.
[5] *School of Earth Science and Engineering*, *Hebei University of Engineering*, *Handan* 056038, *Hebei Province*, *China*.

Abstract: A typical high-temperature metamorphic rock geothermal reservoir was newly discovered in the Tianzhen geothermal field in Datong City, China. However, due to the complex geological structure and thermal properties, the seepage heat transfer mechanism of metamorphic rock reservoirs is still unclear, seriously impeding the efficient development and sustainable utilization of geothermal resources. This study established a percolation-heat transfer model through tracer testing and numerical simulation to reveal the percolation mode and heat transfer mechanism of high-temperature metamorphic rock reservoirs during the reinjection process. We also predicted the distribution characteristics of various physical fields in the geothermal reservoir after the geothermal system has been in operation for 100 a, analyzed the influence of different reinjection schemes on seepage heat transfer in the geothermal reservoir, and proposed an optimization strategy for the reinjection scheme. The results show that: (1) The connectivity between production and injection wells is poor, and there are water-conducting fractures connecting the shallow and bottom layers; (2) The seepage channels through fractures guide the migration of the reinjected fluid and form a cold front surface with a protruding shape towards the mining well in the temperature field, resulting in temperature changes in the production well; (3) Seepage heat transfer in thermal reservoirs is greatly affected by the reinjection flow rate and the distance between production and reinjection wells, but less by the reinjection temperature. As the reinjection temperature drops, the flow rate increases, the well spacing decreases, and the temperature variation range of the production well becomes greater; (4) Under the current reinjection test conditions, the temperature of the mining well decreased by approximately 4°C after 100 a of geothermal reinjection operation, and a thermal breakthrough occurred at 78 a. Under the condition of maintaining a reinjection flow rate of 60 m^3/h and a reinjection temperature of 80°C unchanged, the well spacing should be no less than 470 m to ensure that the well temperature does not cause a thermal breakthrough during the reinjection operation for 100 a. This research provides a theoretical basis and optimization methods for the efficient development of high-temperature metamorphic rock thermal reservoirs.

Keywords: Metamorphic rock; Thermal reservoir; Geothermal reinjection; Seepage law; Temperature field evolution; Optimization strategy

Received: 25 Jan 2025/ Accepted: 16 Feb 2026/ Published: 18 May 2026

*Corresponding author: Yan-guang Liu, Xin Wang, *E-mail address*: gaoyuanzhixing@163.com, wangxin112914@163.com

DOI: 10.26599/JGSE.2026.9280085

Wei MH, Liu YG, Wang X, et al. 2026. Mechanism of seepage heat transfer in thermal reservoirs of high temperature metamorphic rocks in the Yanggao-Tianzhen basin. Journal of Groundwater Science and Engineering, 14(3): 323-341.

2305-7068/© 2026 Journal of Groundwater Science and Engineering Editorial Office This is an open access article under the CC BY-NC-ND license (http://creativecommons.org/licenses/by-nc-nd/4.0)

Introduction

Against the backdrop of the continuous growth of energy demand, geothermal resources, as a sustainable and clean energy source, have broad prospects for development and utilization (Stefansson, 1997; Allen and Milenic, 2003). Geothermal reinjection is an important way to achieve efficient and

sustainable development of geothermal energy. However, long-term geothermal reinjection is prone to cause the temperature of the extraction well to drop and even trigger thermal breakthrough, seriously affecting the heat extraction efficiency of the geothermal system (Cao et al., 2021). For the efficient development and sustainable utilization of geothermal resources, it is necessary to accurately grasp the seepage heat transfer mechanism of thermal reservoirs (Liu, 2003; Wang et al., 2020a; Kamila et al., 2021; Diaz et al., 2016).

Located in the northeastern part of Shanxi Province, the Datong Basin exhibits substantial geothermal resources with a spatially concentrated distribution. Notably, the Yanggao-Tianzhen area displays the most pronounced geothermal anomalies, primarily associated with metamorphic rock thermal reservoirs. Initial geothermal exploration efforts in the 1990s, concentrated in areas such as Maquanxiang (Tianzhen County) and Gushanmiao (Yanggao County) (Pan et al., 2023), led to a preliminary delineation of geothermal field boundaries. Subsequent investigations over the following decades resulted in the discovery of a high-temperature, high-pressure geothermal well in both Yanggao and Tianzhen counties. The DR1 geothermal well in Tianzhen, exhibiting an orifice temperature of 160.2°C and a single-well flow rate of 230 m^3/h, represents the highest temperature and largest self-flowing geothermal well discovered to date in central and eastern China (He et al., 2023). Furthermore, the Paleozoic metamorphic rock geothermal reservoir underlying the Yanggao-Tianzhen Basin is characterized by high thermal conductivity and temperature, coupled with a relatively shallow burial depth, facilitating the potential for large-scale development of high-temperature hydrothermal geothermal resources. Despite the considerable success in geothermal exploration within the Yanggao-Tianzhen area, the immature state of reinjection technology for fractured metamorphic rock reservoirs, compounded by an incomplete understanding of seepage and heat transfer mechanisms, has hindered the scientific, efficient, sustainable, and large-scale development and utilization of these geothermal resources.

The fluid seepage path within a geothermal reservoir exerts a direct influence on the seepage heat transfer process, leading to varied temperature field evolution (Zhou et al., 2022; Du et al., 2019; Tang and Qiu, 2023; Wang et al., 2021; Fan et al., 2023). The inherent heterogeneity of geological features, coupled with complex pore and fracture networks, renders the seepage heat transfer mechanism of geothermal reservoirs under production and injection scenarios intricate and multifaceted, remaining a key area of investigation in geothermal research. Researchers have employed laboratory experiments, field reinjection tracer tests, and numerical simulations to investigate geothermal reservoir seepage heat transfer under reinjection conditions. Laboratory simulations, utilizing scaled-down geothermal reinjection systems, have been used to examine the seepage heat transfer processes within reservoir rocks under varying injection parameters, aiming to characterize the percolation heat transfer properties of small-scale thermal reservoirs (Ma et al., 2019b; Ma et al., 2019a; He et al., 2016; Zhang et al., 2021). These studies have identified rock fracture structure, reinjection conditions, and rock temperature as key influencing factors in the seepage heat transfer process (Huang et al., 2019; Huang et al., 2021). Given that geothermal reservoirs are typically located hundreds or even thousands of meters below the surface, direct observation of fluid migration pathways is not feasible. Field reinjection tests, incorporating tracer technology, provide an important means to study the seepage heat transfer mechanism of thermal reservoirs and optimize exploitation strategies. By introducing tracers and monitoring their response, researchers can infer the seepage heat transfer mechanism in response to different reinjection methodologies (Ren et al., 2023). Tracer concentration response curves, obtained by injecting tracers into geothermal wells, allow for the tracking of fluid flow paths within the reservoir and assessment of connectivity between production and reinjection wells (Wang et al., 2014; Radilla et al., 2012; Aquilina et al., 2004; Wang et al., 2013; Qiao et al., 2023; Li et al., 2020; Liu et al., 2019b; Liu et al., 2022). Advances in tracer technology, including the development of novel geothermal tracers (Bottacin-Busolin et al., 2021), improved monitoring techniques, and sophisticated data analysis and interpretation, provide increasingly valuable information for elucidating the seepage heat transfer mechanisms of geothermal reservoirs, such as heat exchange area and temperature variation (Juliusson and Horne, 2013; Hawkins et al., 2017). The temperature and flow data derived from laboratory simulations and field tests constitute an essential foundation for investigating the seepage heat transfer mechanism within geothermal reservoirs and optimizing on-site reinjection parameters.

The wide application of numerical simulation has become an important means to study the seepage heat transfer mechanism of thermal reservoirs

(O'Sullivan et al., 2001; Luo, 2018; Yu et al., 2023). By taking into account parameters such as the permeability of the formation, porosity, and thermal conductivity of the rock to establish a mathematical model of the heat reservoir, researchers can simulate the seepage characteristics, temperature distribution, and evolution process of the heat reservoir under different reinjection conditions. These simulation results provide important references for understanding the seepage heat transfer mechanism of thermal reservoirs. They also provide a scientific basis for optimizing the geothermal exploitation plan (Wang et al., 2021; Liu et al., 2020; Yao et al., 2022; Zheng et al., 2022; Liu et al., 2019a). Therefore, regulating the reinjection mode and optimizing the layout of geothermal wells through the seepage heat transfer mechanism of the thermal reservoir can achieve the purpose of prolonging the service life of geothermal Wells and improving the extraction efficiency and economy of geothermal energy (Wang and Lu, 2023; Kuo et al., 2018).

This study focused on the high-temperature metamorphic rock geothermal reservoir in the Tianzhen Geothermal Field, Datong City, China. We conducted reinjection tracer tests and developed a wellbore-reservoir coupled seepage-heat transfer model utilizing COMSOL software. By integrating the tracer test results with numerical simulation, we elucidated the seepage behavior and heat transfer mechanisms within the metamorphic rock geothermal reservoir during reinjection. In addition, we predicted the distribution characteristics of various physical fields of the geothermal reservoir during the 100 a reinjection cycle, and studied the influence of different reinjection parameters such as reinjection temperature, flow velocity, and well spacing on the temperature field of the thermal reservoir. Based on these analyses, we proposed an optimized geothermal reinjection strategy and assessed the inherent uncertainties in the research. Ultimately, this work aims to provide a robust theoretical foundation and valuable technical support for the efficient exploitation and sustainable management of geothermal resources.

1 Regional geological overview

1.1 Regional structure

The geothermal field for this experiment is located in the northern part of Shuitongsi Village, Guqianbao Town, Tianzhen County, Datong City, Shanxi Province, China, situated in the Yanggao-Tianzhen Basin in the northeastern part of the Datong Basin (Fig. 1). Geologically, this area belongs to the Yanggao-Tianzhen block of the active belt on the northern margin of the North China Plate, generally extending in a NEE direction (Shi et al., 2015). The Datong Basin, situated at the junction of the central and western parts of the North China Craton, is a Cenozoic faulted basin in the central North China Block. Since the Late Mesozoic, it has experienced multiple tectonic events and sustained intense extensional activities, resulting in localized lithospheric modification and thinning. Consequently, a series of step-like extensional normal faults have formed, creating grabens and half-grabens (Li et al., 2012; Shi et al., 2015). These grabens and basin-margin controlling faults collectively form a NE-SW trending half-graben basin. The basin's formation is primarily controlled by boundary faults, with internal tectonic activities being mainly inherited faults, followed by folds, with a predominant NE tectonic direction. The main boundary faults are illustrated in Fig. 1b: Kouquanshan Fault (F1) trends NNE, while Liulingshan Fault (F2), Hengshan Fault (F3), Yunmenshan Fault (F4), Xionger Mountain north margin Fault (F5), Xionger Mountain south margin Fault (F6), and Xiaowutai Mountain Fault (F7) all trend NEE. Additionally, there are concealed faults in the area (Cen et al., 2015).

1.2 Geothermal geological conditions

The study area is divided into two main thermal reservoir series from top to bottom: The Cenozoic loose rock thermal reservoir and the Neoarchean metamorphic rock thermal reservoir. The upper thermal reservoir is covered by Neogene and Quaternary strata, primarily formed by the accumulation of alluvial sediments since the Cenozoic era. The lithology consists mainly of gravel sand, sand, and silt, with a dark yellow color and a thickness of about 100–300 m. Below it lies the Neoarchean Jining Group metamorphic thermal reservoir, characterized by biotite plagioclase gneiss, amphibolite, and monzonitic gneiss. The overall temperature distribution of the thermal reservoirs in the study area ranges from 167°C to 181°C, and the hydrochemical type is $Cl{\cdot}SO_4$-Na type.

The geothermal heat source in the study area primarily originates from two aspects. Firstly, the Datong Basin corresponds to the destruction of the craton in western North China, resulting in asthenospheric upsurge and mantle thermal erosion (Liu et al., 2004). Mantle activity transfers heat to the crust. Under the action of plate compression,

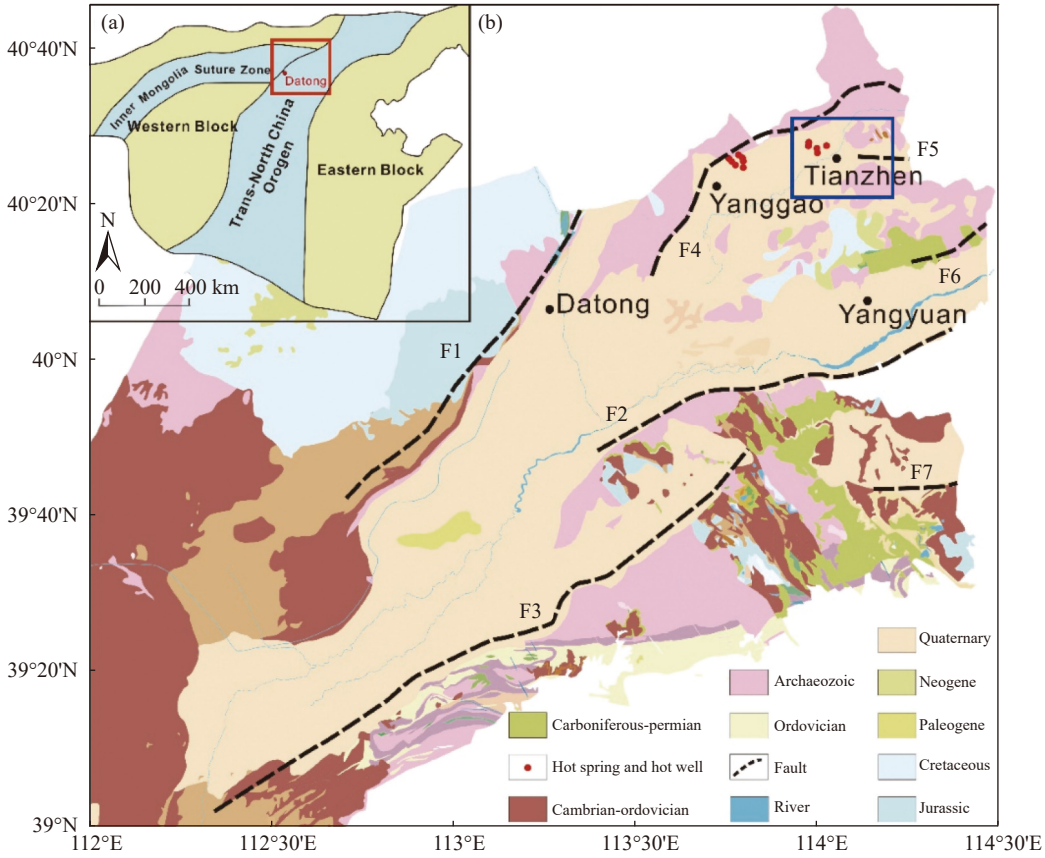


Fig. 1 (a) Location of the North China Craton, with a red box indicating the Datong Basin; (b) Tectonic background of the Datong Basin (blue box indicating the study area) (Kusky and Li, 2003; Zhou et al., 2020)

the crust is thickened and decompressed, leading to the dehydration of molten crust and the formation of partial melt, which continuously supplies heat through conduction (Zhu et al., 2012). Secondly, the Datong Basin is situated at the boundary of block activity and is a region of continental crust spreading and cracking. As the crust thinned, shallow-buried magma was ejected to the surface due to neotectonic movements, forming the Datong volcanic group. The magma that did not reach the surface migrated along crustal fissures towards the NE direction of the basin. Under tectonic stress, an upward semi-molten magma sac is formed, transferring heat to the shallow surface along the fractures. The shallow surface geothermal heat is transferred in the form of convection under the atmospheric precipitation supply, which provides a stable heat source for the formation of geothermal resources in the study area (Zhou et al., 2020).

1.3 Distribution of geothermal Wells in the study area

The test site contains four deep-hole geothermal wells: GR1 (Depth 1,624.01 m), DR1 (Depth 1,759.21 m), DR2 (Depth 3,112.72 m), and HG1 (Depth 3,007.25 m), along with five shallow temperature-measuring wells: K4 (Depth 306.77 m), K6(Depth 321.29 m), K11 (Depth 329.01 m), K13 (Depth 314.87 m), and K18 (Depth 151.34 m). Their locations are shown in Fig. 2. Well DR1 is situated approximately 69° west of well GR1, with a distance of 440 m between them. Well DR2 is positioned about 20° west of well GR1, at a distance of 1,042 m. Well HG1 is located approximately 71° east-northeast of well GR1, with a spacing of 1,290 m.

The reinjection test adopts same-layer reinjection. GR1 is a production well, with the bare well section ranging from 1,502.82 m to 1,624.01 m. The main lithology of the thermal reservoir around the well is the Neoarchean Heiyun II gneiss, interspersed with Feili porphyry dykes. The highest temperature in the production well was 167.94°C (Fig. 3). DR1, as a reinjection well, has a bare well section ranging from 1,188.29 m to 1,759.21 m. The main lithology of the thermal reservoir around the well is the Neoarchean Black Cloud diorite gneiss, interspersed with plagioclangle rocks and diorite granites, etc. The highest temperature in the reinjection well is 169.0°C.

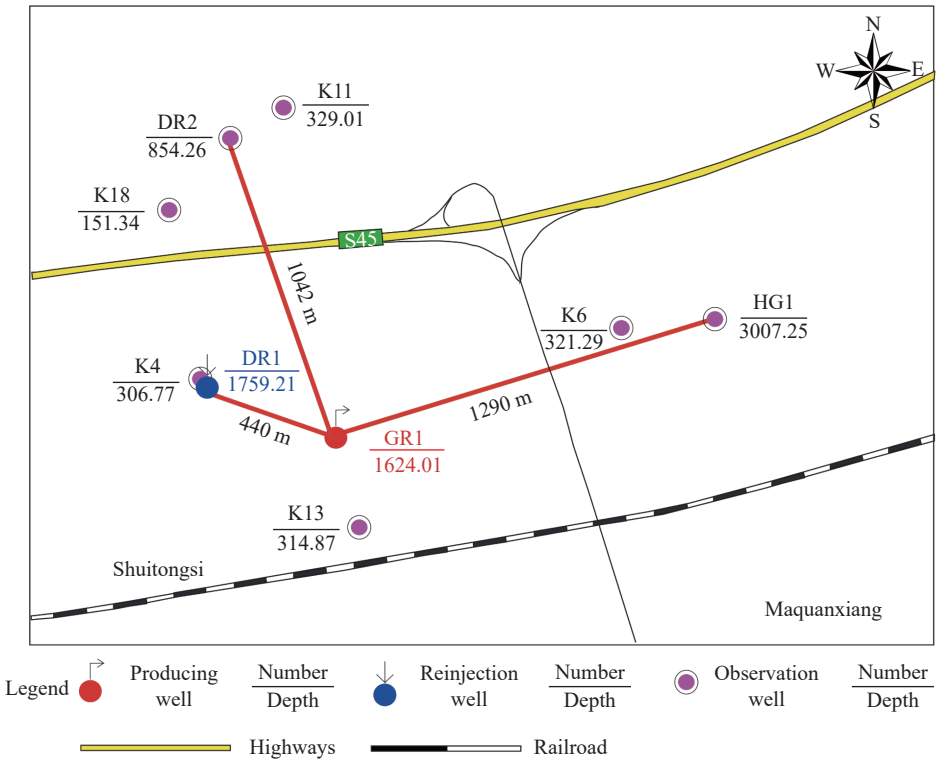


Fig. 2 Distribution of well locations in the study area

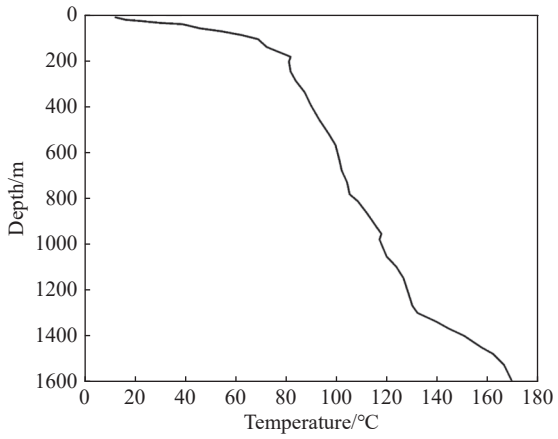


Fig. 3 Temperature measurement curve of well GR1

2 Field tracer test method

2.1 Tracer selection

After thoroughly investigating the physical and chemical properties of the tracer and its background value in the study area, sodium 1,5-naphthalene sulfonate was chosen as the test tracer. Rose et al. (2001) indicates that naphthalene sulfonate possesses thermal stability below 330°C, is cost-effective, non-toxic, environmentally benign, and easily detectable by High-Performance Liquid Chromatography (HPLC) and ultraviolet absorbance, with an excellent detection limit of less than 0.1 ppb, making it a suitable high-temperature geothermal tracer (Rose et al., 2001). Naphthalene sulfonates have been employed in most geothermal fields worldwide (Rose et al., 2012). Before the tracer test, a tracer adsorption experiment was conducted. The prepared 1, 5-naphthalene sulfonate standard solution and metamorphic rock debris collected from the study area were tested using a high temperature and high-pressure reactor, and detection was performed using a high-performance liquid chromatography system. The results demonstrated that 1,5-naphthalene sulfonate exhibited good water solubility and did not adsorb onto the rocks in the study area at high temperatures, meeting the requirements for tracer selection.

2.2 Tracer dispensing and sampling detection

Prior to releasing the tracer, the amount of tracer was estimated, and the background levels of the tracer in the production well GR1, the reinjection well DR1, and the surrounding observation wells were investigated. According to the NB/T10703-2021 technical regulations for thermal reservoir tracer test, tracer release amounts can be calculated according to Equation (1):

$$G = \pi R^2 H \alpha \beta C_p \quad (1)$$

Where: R is distance between injection well and

production well (m), 440; H is thickness of the thermal reservoir, based on the length of the water intake section of the geothermal well (m). This time, the length of the bare well section of production well GR1 is taken as 120; α is the dispersion constant factor, generally 0.0153; β is the dominant flow concentration field correction coefficient, generally 0.1; Cp is the peak tracer concentration (kg/m^3); G is the tracer dose.

The peak concentration of the tracer is two orders of magnitude higher than the background value in the local natural groundwater. According to Equation (1), the dosage is calculated to be 370 kg. To ensure that the tracer can be effectively detected in the test, 1.5 times the designed value is taken as the injection amount for the geothermal well, that is, 550 kg.

The reinjection trial commenced on July 20, 2023. During the test, the reinjection rate of well DR1 was 60 m^3/h, and the production rate of well GR1 was also 60 m^3/h, resulting in production-reinjection ratio of 100%. At the beginning of the test, the reinjection pressure was 0.645 MPa, and during the test, the reinjection pressure remained stable at 0.664–0.686 MPa. After two weeks of operation of the geothermal reinjection system, tracer (sodium naphthalene sulfonate) was injected into the reinjection well DR1 on August 4, 2023. Following the tracer reinjection, water samples are collected from production wells using multistage sampling. Initially, water samples were taken every half hour for the first month, then the frequency was gradually reduced to every 2 hours, every 4 hours, every 8 hours, every 10 hours, and every 12 hours over two weeks. After 86 d, the sampling interval was further reduced to once every 20 d. The final reinjection tracer test lasted for a total of 160 d. Additionally, samples from observation wells around the test site were collected every 10 d.

The tracer detection of water samples collected in the experiment was completed by the laboratory of Geothermal and Dry Hot Rock Exploration and Development Technology Innovation Center of the Ministry of Natural Resources, and the detection was carried out by Agilent high- performance liquid chromatography. The system has high sensitivity, is not easily polluted, and has the advantages of low cost and simple operation. The detection limit of sodium naphthalene sulfonate is 1.0×10^{-9} mol/L.

2.3 Tracer transport theory

In the equivalent seepage channel model of deep thermal reservoirs, it is assumed that there are several favorable seepage channels (such as fracture zones) between the reinjection well and the production well. These channels dominate the flow process of the reinjection water migrating from the reinjection well to the production well and maintain a stable flow rate (Zhao et al., 2021). The flow in this process can be approximately equivalent to Darcy flow. Suppose the geometry of the channel is rectangular, with a length much larger than the opening and height (Fig. 4).

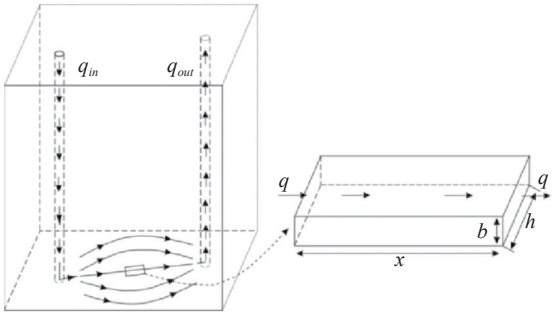


Fig. 4 Schematic diagram of the seepage channel model of a deep thermal reservoir (Li et al., 2020)

The migration of tracers is mainly achieved through convection and hydrodynamic diffusion, and is independent of the adsorption effect of heat sources. Ignoring the molecular diffusion effect and combining it with the law of conservation of tracer mass, the expression of tracer mass concentration in production wells can be expressed as:

$$c(t)=\frac{\rho_w M\mu}{2Q\sqrt{\pi Dt}}e^{\left(-\frac{(x-\mu t)^2}{4Dt}\right)} \tag{2}$$

Where: $c(t)$ is the tracer concentration of the reinjection water at the crack outlet (kg/m^3); ρ_w is the density of reinjection water (kg/m^3); M is the tracer dose (kg) flowing into the seepage channel; μ is the movement velocity of reinjection water in the fissure (m/s); Q is the production rate (kg/s); D is the dispersion coefficient (m^2/s); t is time (s); x is the length (m) of the fissure channel between the reinjection well and the production well.

If there are n flow channels between the reinjection well and the production well, the tracer concentration expression in the production well is

$$c(t)=\sum_{i=1}^{n}c_i(t) \tag{3}$$

$$c_i(t)=\frac{\rho_w M_i\mu_i}{2Q\sqrt{\pi D_i t}}e^{\left(-\frac{(x-\mu t)^2}{4Dt}\right)} \tag{4}$$

$$\mu_i=\frac{q_i}{\rho A_i\varphi_i} \tag{5}$$

$$q_i = \frac{M_i}{M} q_{in} \tag{6}$$

$$D_i = \alpha L_i \mu_i \tag{7}$$

In Equations (3)-(7), $c(t)$ is the tracer concentration in the production well (kg/m^3); n is the number of dominant fracture channels; ρ_w is the water density (kg/m^3); m_i is the mass (kg) of the tracer flowing through the i fracture channel. x_i is the length of the i fracture channel (m); Q is the extraction rate (kg/s); t is the time (s); D_i is the longitudinal dispersion coefficient (m^2/s) in the i fissure channel; μ_i is the flow velocity in the i fracture channel (m/s); q_i is the reinjection rate in the i fracture channel (kg/s); A_i is the cross-sectional area of the i fracture channel (m^2); φ is the porosity (%); αL_i is the longitudinal dispersion (m) in the i fissure channel; M is the mass of the tracer input (kg); q_{in} is the reinjection rate (kg/s).

In Equation (6), M_i/M is often referred to as the tracer recovery rate. In theory, the tracer recovery should be 100% when there is no environmental flow and the tracer does not interact with the thermal reservoir. In fact, the diffusion and dispersion of tracers in the thermal reservoir matrix are two major factors that lead to reduced recovery rates (Sanford et al., 2006). Instantaneous moment analysis was used to evaluate the tracer recovery to verify the characteristics of the tracer in the experiment (Rose et al., 2004). The tracer recovery mass M_i is calculated by the following formula.

$$M_i = Q_P \int_0^t C(t)\, dt \tag{8}$$

Where: Q_p is the pumping rate (kg/s), $C(t)$ is the tracer concentration (kg/m^3) and t is the time (s).

According to Equation (2), $C(t)$ can be detected by tracer tests, while there are many unknowns on the right side of the equation, such as the cross-sectional area of the channel and the longitudinal dispersion cannot be directly measured. In this paper, ICEBOX program was used to invert the tracer test results to evaluate the tracer recovery and temperature change in the seepage channel (Axelsson et al., 2005).

3 Numerical simulation method

Numerical simulation is crucial for geothermal resource assessment, optimal design of reinjection schemes, and thermal breakthrough prediction in geothermal wells. In this study, COMSOL Multiphysics, a mature finite element calculation software for geological body multi-field coupling, was used for modeling. Previous studies have demonstrated the reliability of COMSOL in the calculation of seepage heat transfer and solute transport problems (Liu et al., 2019b; Zinsalo et al., 2020; Shi et al., 2023). The flow, heat transfer, and tracer transport processes in thermal reservoirs and fractures are considered, utilizing physical fields such as Darcy's law, heat transfer in porous media, transfer of matter in porous media, and heat transfer in pipelines. Based on the equivalent seepage channel model (Fig. 4), the thermal reservoir bedrock is treated as a porous medium rich in pores, with long fractures forming the equivalent seepage channels that direct the reinjection water. The geothermal well structure is simulated using one-dimensional line elements (Al-Khoury et al., 2005; Al Khoury and Bonnier, 2006). Fluid flow in geothermal reservoirs conforms to Darcy's law and is governed by the mass conservation equation. The heat transfer process in the thermal reservoir includes the heat conduction between rocks and the heat convection effect of fractures, which can be described by the energy conservation equation. Combined with the tracer transport theory, the transport process of tracers in thermal reservoirs and fractures can be described by the classical convection-diffusion equation in porous media. The equations of each physical field are shown in Table 1 (Wang et al., 2020b; Cui et al., 2018; Liu et al., 2019a; Pandey et al., 2018).

3.1 Model building and meshing

Based on the above numerical simulation method and in accordance with the distribution of geothermal wells and the geothermal geological conditions in the study area, a geothermal well numerical model with a planar size of 1,500 m × 1,000 m and a depth of 2,000 m was established (Fig. 5a). The model includes a geothermal field, two layers of thermal reservoirs, two geothermal wells and a fissure channel. The initial pressure of the model is set according to the hydrostatic pressure of the reservoir. The top and bottom of the model are set as no-flow boundaries, and the side boundaries around the model are set as water head boundaries. After the reinjection begins (t>0), a flow boundary is set for the bare well section within the thermal reservoir. The initial temperature field of the model was set based on the geothermal gradient of the study area and the temperature measurement curve of well GR1. The top of the model was set to a fixed surface temperature (20°C), the bottom was set to thermal insulation, and the four sides were

Table 1 Governing equations for each physical field

Description	Governing equation
Seepage equations in thermal reservoirs	$\frac{\partial}{\partial t}(\rho_{\mathrm{f}}\varphi)+\nabla\cdot(\rho_{\mathrm{f}}\mathbf{u}_{\mathrm{f}})=Q_{\mathrm{m}}$
Heat transfer equation in thermal reservoir	$(\rho C_p)_{\mathrm{eff}}\frac{\partial T}{\partial t}+\rho_{\mathrm{f}}C_{\mathrm{p,f}}\mathbf{u}_{\mathrm{f}}\cdot\nabla T-\nabla\cdot(k_{\mathrm{eff}}\nabla T)=q_f$
Solute transport equations in thermal reservoirs	$\frac{\partial C}{\partial t}=D\frac{\partial^2 C}{\partial x^2}-u\frac{\partial C}{\partial x}$
Heat transfer equation of wellbore	$\rho_{\mathrm{f}}A_{\mathrm{w}}C_{\mathrm{p,f}}\frac{\partial T}{\partial t}+\rho_{\mathrm{f}}AC_{\mathrm{p,f}}\bar{u}_{\mathrm{w}}\cdot\nabla T=\nabla\cdot Ak\nabla T+f_{\mathrm{D}}\frac{\rho_{\mathrm{f}}A}{2d_{\mathrm{i}}}\lvert u\rvert^3+Q_{\mathrm{wall}}$

Notes: Where: t is time (s), ρ_{f} is the fluid density (kg/m^3), Q_m is the fluid mass source (kg/(m^3·s)), $C_{\mathrm{p,f}}$ is the specific heat capacity of the fluid under constant pressure (J/kg/K), T is the temperature (K), q_f is the heat source (W/m^3), and $(\rho Cp)_{eff}$ is the equivalent volumetric heat capacity of the reservoir rock mass k_{eff} is the effective thermal conductivity of the reservoir rock mass (W/m/K), C is the tracer concentration/(kg/m^3); t is time (s), x is the channel axial coordinate (m); D is the tracer axial dispersion coefficient (m^2/s); u is the average flow rate of the fluid (m/s); A_w is the cross-sectional area of the geothermal well (m^2); u_w is the average flow velocity along the shaft axis (m/s); Q_{wall} is the heat exchange between the fluid and the surrounding rocks through the geothermal well wall, and f_{D} is the Darcy friction factor.

set to open boundaries. For the solute transport process, the initial concentration of the model is 0. Flux-free boundaries are set at the top and bottom, and open boundaries are set on the four sides. After the reinjection begins, a line mass source boundary is set in the bare well section of the thermal reservoir. The reinjection parameters in the model are taken based on the on-site reinjection tracer test values as shown in Table 2. The reinjection temperature and flow rate are both set according to the parameters during the on-site tracer test. The parameters of the thermal reservoir were obtained based on on-site test results.

3.2 Meshing and sensitivity analysis

To ensure the accuracy of the numerical simulation, a sensitivity verification of grid division was carried out. In COMSOL, free tetrahedral meshes are respectively applied to the solid matrix and the fracture channels, and the meshes near the frac-

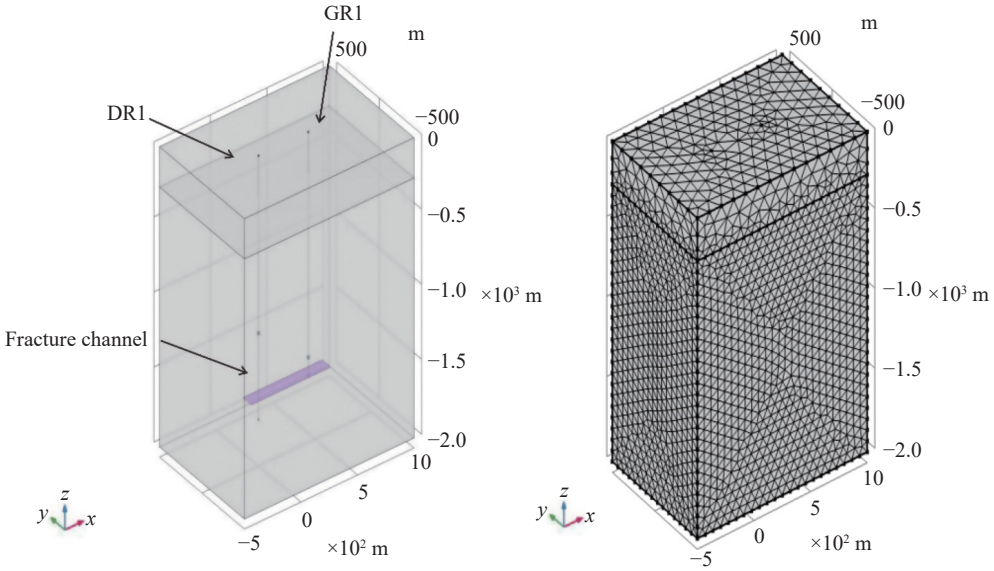


Fig. 5 Numerical model diagram (a) and meshing diagram (b)

Table 2 Model parameter table

Parameters	Value	Parameters	value
Reinjection temperature	80°C	Reservoir density	2,689 kg/m³
Thermal reservoir temperature	169°C	Reservoir porosity	2.5%
Reinjection flow	60 m^3/h	Thermal conductivity of reservoir rock	7 W/(m·K)
Fluid density	1,000 kg/m³	Reservoir permeability	2×10^{-16} m^2
Fluid heat capacity	4,200 J/(kg·°C)	Reservoir heat capacity	920 J/(kg·°C)

tures are refined. The grids are divided respectively in refined, ultra-refined and extremely refined modes. By calculating the peak concentration of tracer in the production well (t = 40 d), models with different grid numbers were compared (Table 3). When the number of grids was increased, the peak changes in the tracer concentration of the production wells were all less than 0.1%. In this study, the model adopted ultra-fine grid division to avoid grid effects and ensure the accuracy of the calculation results, as shown in Fig. 5b.

Table 3 Grid sensitivity analysis

Grid division mode	Number of grids	Calculate the peak concentration of tracer in the mining well (t = 40 d) ($\times10^{-3}$/m^3)
Refine the mesh	46,371	1.4525
Ultra-fine grid	135,351	1.4523
Extremely fine grid	224,470	1.4519

3.3 Numerical model validation

The variation curve of tracer concentration in the bare well section of the production well during the test period was calculated by the transient solution method and compared with the analytical Equation (2) and the on-site tracer test results to verify the applicability of the model (Fig. 6). The results show that the tracer concentration curve calculated by the model conforms to the changing trend of the tracer response curve and fits well with the analytical Equation (2) and the on-site tracer test data, indicating that the numerical model can approximately reflect the seepage heat transfer and tracer migration processes in the thermal reservoir within the study area.

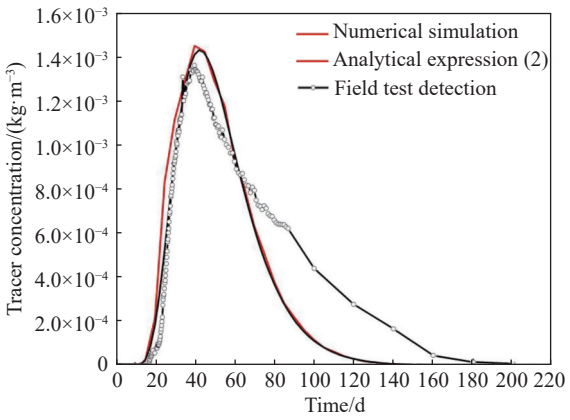


Fig. 6 Numerical simulation results, analytical Equation (2), and on-site test results

4 Results and discussion

4.1 Tracer breakthrough curve and temperature variation

Tracer concentrations in collected water samples were analyzed to generate a time-series scatter plot illustrating the relationship between tracer concentration and water temperature in geothermal well GR1 (Fig. 7). The tracer was initially detected 15 d after reinjection, with concentrations subsequently increasing. Following 20 d, the concentration exhibited a gradual rise, peaking around day 40 and remaining elevated for two d before a gradual decline. The decrease in tracer concentration demonstrated a slow and protracted tailing effect. Due to the limitations of the on-site conditions, the sampling density was reduced to once every 20 d after 86 d of the tracer test, and it ended after 160 d of the reinjection tracer test. Continuous temperature monitoring of the production well revealed an overall temperature fluctuation of less than 1°C during the test period. Notably, a sharp temperature change coincided with the tracer's first arrival time at approximately 20 d. Low levels of the tracer were detected in observation wells K4, K6, and K13 (Table 4), with concentrations one to two orders of magnitude lower than those in well GR1. Over time, the tracer concentration in these observation wells generally exhibited a decreasing trend.

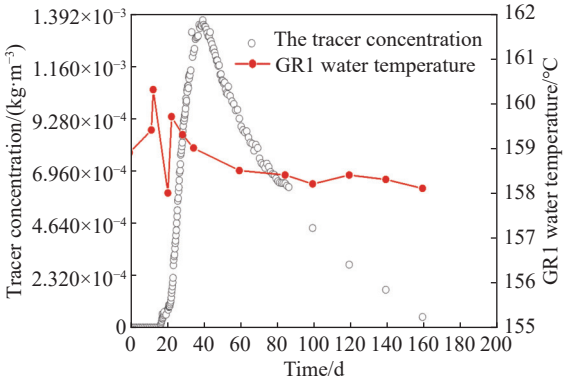


Fig. 7 Tracer concentration detection (left axis) and temperature detection (right axis) in well GR1

4.2 Simulation results of thermal reservoirs

Fig. 8 shows the distribution of thermal reservoir tracers during the test period. The tracer is injected from the reinjection well into the fractured-network thermal reservoir, accompanied by the migration of the reinjection fluid in the thermal reservoir. Under the influence of the seepage and

Table 4 Tracer concentration statistics of observation wells and well GR1

Time(d)	Tracer concentration by well ($\times10^{-6}$ kg/m^3)			
	K4	K6	K13	GR1
8	8.10	50.34	24.82	Tracer was not detected
16	13.39	49.42	12.95	Tracer was not detected
26	28.07	29.00	17.17	480.24
42	10.05	21.16	12.09	1,320.08
61	9.93	23.90	11.23	890.88
69	12.85	16.84	10.90	809.68
78	10.25	15.45	12.30	679.76
86	10.58	13.50	11.23	621.76

distribution diffusion of geothermal fluids, the tracer migrates to the periphery along the pores and fractures in the thermal reservoir. The tracer forms an irregular tracer halo around the reinjection well. Over time, the tracer halo around the reinjection well gradually disappears and diffuses within the thermal reservoir. Some tracers flow along the seepage channels to the mining well under the drive of seepage. This is consistent with the changes in tracer concentration obtained from the field tracer test.

Based on the numerical model, the distribution characteristics of each physical field of the geothermal system after 100 a of operation were predicted. Figs. 8 and 9 respectively show the distribution of the pressure field and seepage field in the thermal reservoir. The pressure at the reinjection well is relatively high, while that at the production well is relatively low. The flow velocity of the reinjected fluid around the well is relatively high and much greater than that of the fluid in the thermal reservoir matrix. The flow of the reinjected fluid, driven by the pressure difference, flows towards the production well or around the thermal reservoir in different directions, with only a small portion flowing towards the mining well

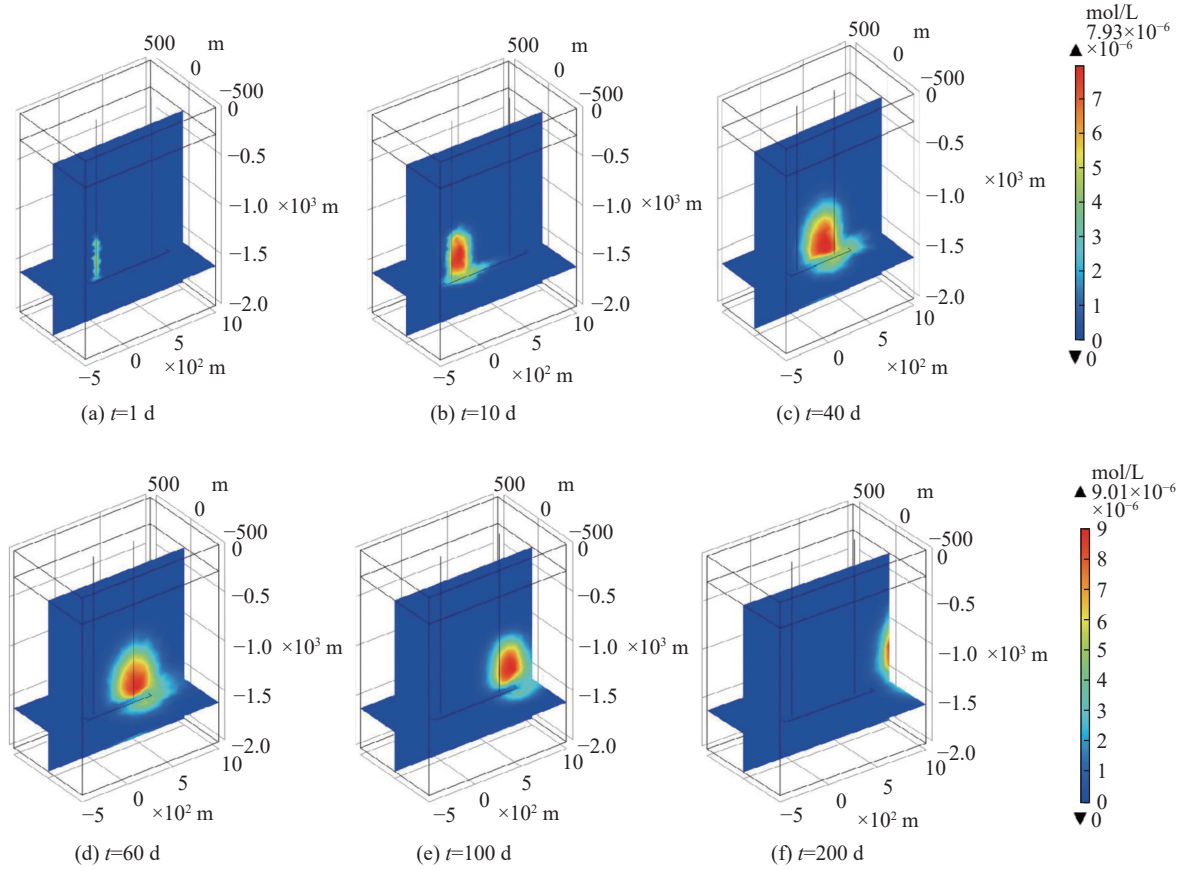


Fig. 8 Variation of tracer concentration at different times in the model

along the connected seepage channels.

The low-temperature tailwater injected into the hot reservoir continuously absorbs heat through rock heat conduction and convection between cold and hot fluids, thereby disrupting the original thermal equilibrium of the reservoir. Over time, the temperature distribution within the hot reservoir influenced by the low-temperature tailwater changes continuously (Fig. 11). Fig. 11 illustrates the temperature field distribution of the thermal reservoir as predicted by the numerical model at various operational times of the geothermal well system. Initially, when the thermal reservoir was undeveloped, the temperature field remained in a relatively stable state of thermal equilibrium, primarily governed by the geothermal gradient and geological structure (Fig. 11a). With the reinjection of low-temperature tailwater, the area around the reinjection well absorbs heat first, leading to a temperature decrease and the formation of a distinct low-temperature zone (Fig. 11b). As the geothermal well system continues to operate, this low-temperature zone expands, and the cold front advances towards the production well due to the combined effects of production and injection. The presence of fracture channels causes some low-temperature water to flow directly to the production well, resulting in uneven fluid flow velocities

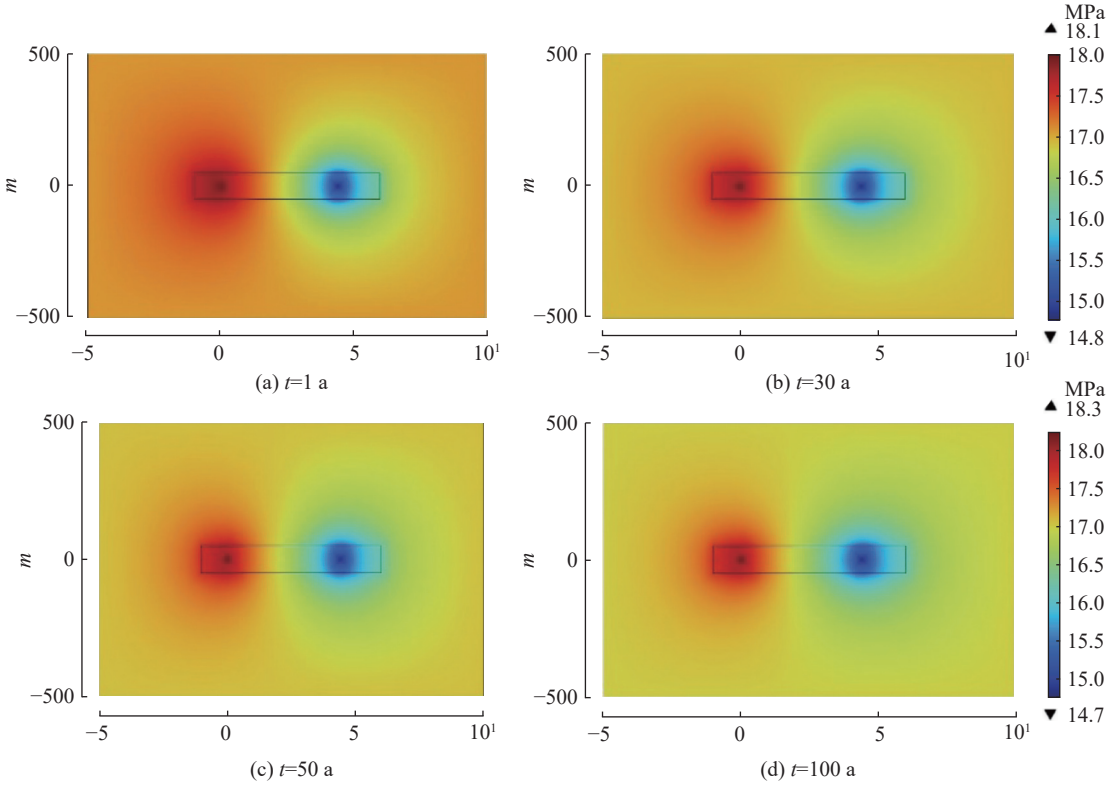


Fig. 9 Pressure field of the thermal reservoir at different times

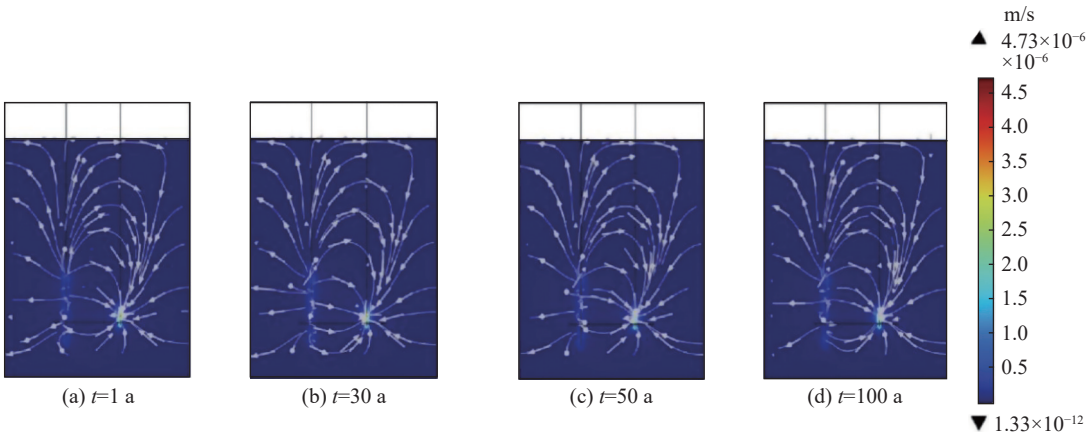


Fig. 10 Seepage field of the thermal reservoir

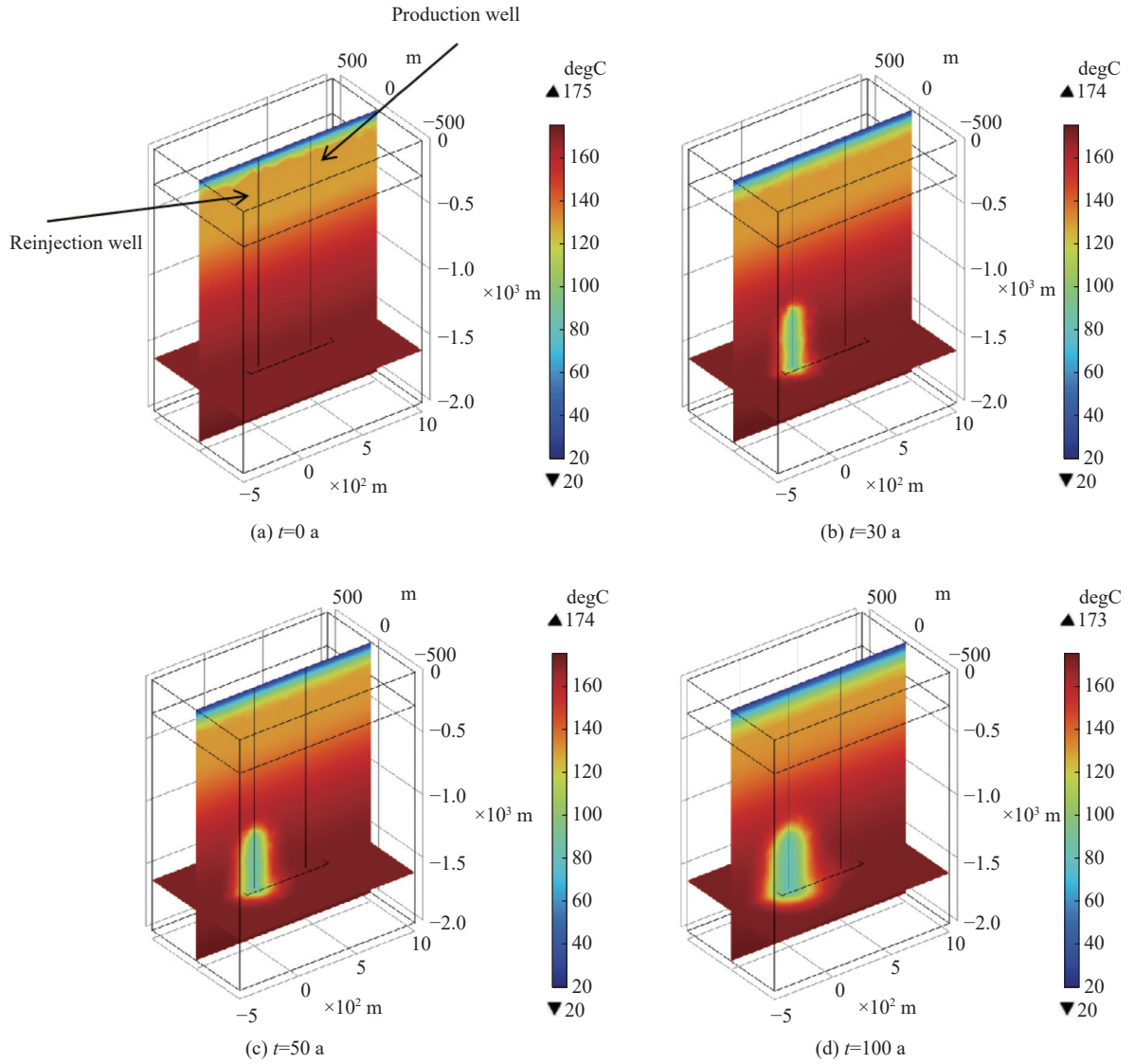


Fig. 11 Temperature field of the thermal reservoir at different times

within the thermal reservoir; the fluid velocity in fractures is faster than in the reservoir matrix. Consequently, the low-temperature water in fractures does not have sufficient time to be heated, leading to a more rapid temperature change in the vicinity of fractures compared to the reservoir matrix (Fig. 11c). With the operation of the geothermal well, the range of the low-temperature zone continuously expands. The cold front surface of the temperature field around the fracture first causes the temperature of the mining well to drop. At t = 100 a, the average temperature of the production well decreased by 4°C compared with the initial value (Fig. 11d). This affects the effective development life and energy recovery efficiency of the thermal reservoir.

4.3 Analysis of seepage path

To address the seepage characteristics of geothermal fluid in thermal reservoirs and subsequently optimize their development and management, tracer technology is often employed. This technique identifies the flow path and velocity of geothermal fluids within geothermal wells or well groups (Axelsson et al., 2005). As illustrated in Fig. 7, the tracer concentration exhibits only one peak, indicating a dominant seepage channel between wells DR1 and GR1. The tracer recovery mass M_i was calculated to be 83 kg by inversion through Equation (8). As the total dosage M of the tracer in the tracer test was 550 kg of tracer, the calculated tracer recovery rate M_i/M was 15.1%. Utilizing the parameters of the thermal reservoir and reinjection (Table 2) along with the tracer recovery rate, the ICEBOX program was employed to invert and fit the parameters of the dominant seepage channel. The longitudinal dispersion of the tracer, the length of the seepage channel, the cross-sectional area of the channel, and the average

migration rate of geothermal fluid derived from the inversion are presented in Table 5.

Table 5 Seepage channel parameter table

Parameter	Inversion result
Tracer recovery rate	15.1%
Channel length	468 m
Seepage velocity	11.6 m/d
Longitudinal dispersion	35 m
Dispersion coefficient	0.00413 m^2/s
Channel cross-sectional area	7.91 m^2

The complete reinjection of extracted geothermal water back into the reservoir, maintained at a 100% reinjection rate via pipeline connections, allows the tracer recovery rate to serve as an indicator of tracer losses resulting from dispersion within the fracture network of the metamorphic rock reservoir. The low recovery rate suggests a highly heterogeneous fracture network within the Yangtian Basin's high-temperature metamorphic rock reservoir, characterized by limited connectivity between production and reinjection wells. Given the Northeast-East (NEE) orientation of the primary fault in the Yangtian Basin, we hypothesize that the dominant fracture direction within the deep metamorphic rock reservoir also aligns with the NEE direction. As the reinjection well is located northwest of the production well, the injected tracer may preferentially flow along these northeast-oriented water-conducting fractures, with only a minor portion reaching the production well. Tracer detection in the surrounding observation wells revealed trace amounts in three shallow wells (K4, K6, and K13), indicating the potential presence of deep fractures or secondary fracture zones within the reservoir that create pathways connecting the deep and shallow formations. These pathways may facilitate the seepage of reinjection water from the deep reservoir to the shallow subsurface, thus accounting for the tracer presence in these shallow wells.

The tracer transport patterns illuminate the seepage pathways of the reinjected water. Based on the preceding analysis, a schematic representation of the seepage channel between the production and reinjection wells was developed (Fig. 12). This depiction suggests that only a small fraction of the reinjected fluid flows towards the production well along the fracture-dominated seepage channel, while branching flows diverge from this main path. A large amount of reinjection fluid may flow in the northeast direction or other directions, and a small portion of the reinjection fluid may seep into the shallow strata along the water-conducting fractures in the reservoir.

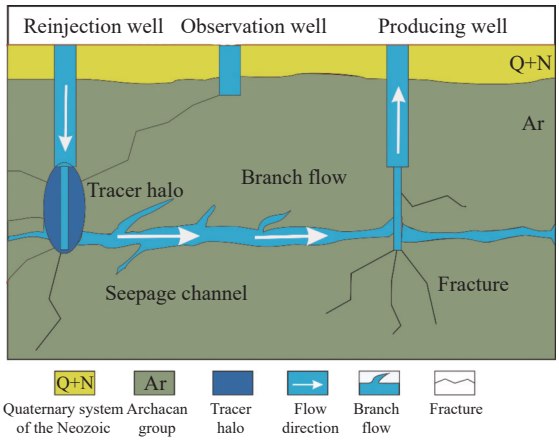


Fig. 12 Prediction of seepage pathways between production and reinjection wells

4.4 The influence of reinjection schemes on seepage heat transfer in thermal reservoirs

To study the influence mechanism of reinjection schemes on seepage heat transfer in thermal reservoirs, the current reinjection schemes were evaluated through numerical models, so as to formulate the optimal reinjection scheme and improve the heat extraction efficiency and safety of geothermal exploitation. Based on the parameters of the thermal reservoir and geothermal well in Table 2, the average temperature variation of the production well under different reinjection schemes was simulated (Fig. 14). For details, please refer to the parameter value table of the reinjection scheme (Table 6).

Fig. 13a illustrates the impact of varying reinjection temperatures on the average temperature evolution of the production well, maintaining a constant reinjection flow rate (60 m^3/h) and well spacing (440 m). Specifically, with reinjection temperatures of 25°C, 50°C, and 80°C, the average production well temperatures after 100 a of geothermal system operation are 163.7°C, 164.5°C, and 165.6°C. Lower reinjection temperatures are associated with earlier temperature impact on the production well and a larger temperature variation range after a century of operation. This phenomenon is attributable to the increased temperature differential between the lower-temperature injected fluid and the surrounding high-temperature rock, which enhances heat transfer efficiency. Consequently, the fluid extracts a

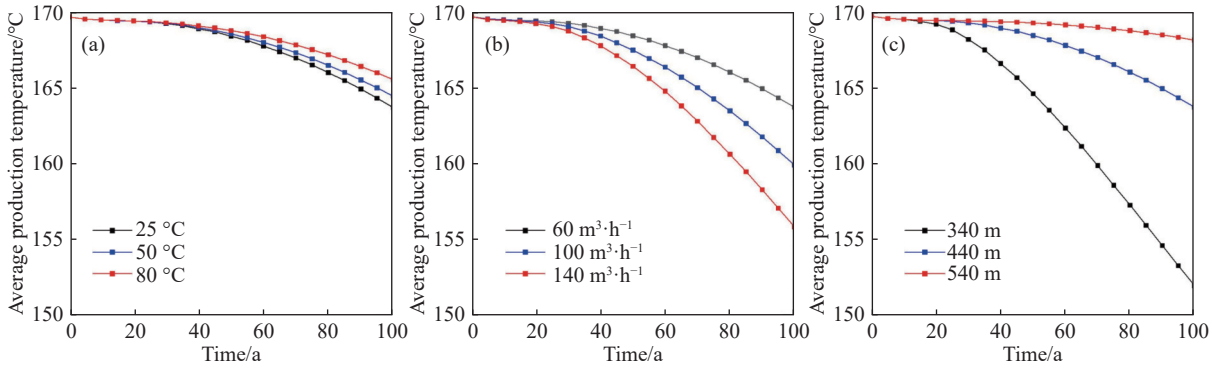


Fig. 13 Average temperature variation of production well under different reinjection schemes

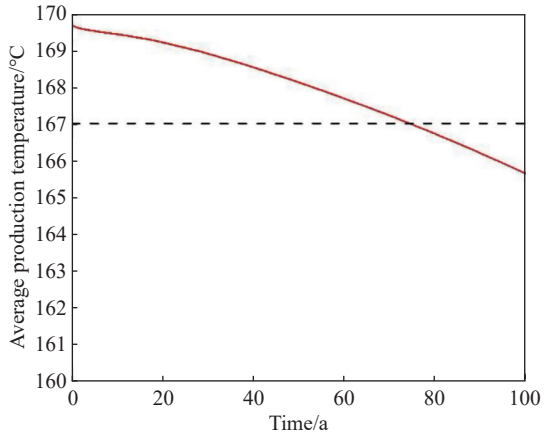


Fig. 14 Temperature change of the production well over 100 a

Table 6 Parameter description of the reinjection scheme

Parameter/unit	Value
Reinjection temperature/°C	25
	50
	80
Reinjection flow/(m^3/h)	60
	100
	140
Production and reinjection well spacing/m	240
	440
	640

greater quantity of heat from the rock mass, leading to an accelerated temperature decline at the production well.

Fig. 13b illustrates the impact of varying reinjection flow rates on the average temperature of the production well, given consistent reinjection temperature (25°C) and well spacing (440 m). Specifically, with reinjection flow rates of 60 m^3/h, 100 m^3/h, and 140 m^3/h, the average production well temperatures after 100 a of geothermal system operation were 163.7°C, 159.9°C, and 155.8°C, respectively. These results indicate an inverse relationship between reinjection flow rate and both the time to thermal breakthrough and the average production well temperature. A higher reinjection flow rate accelerates the arrival of cooler reinjection water at the production well and leads to a greater temperature reduction after a century of operation. The increased flow velocity associated with higher reinjection rates enhances thermal convection, reducing the residence time of the reinjection fluid within the geothermal reservoir. This diminished contact time limits the heat transfer process, resulting in the reinjection water being heated to a temperature lower than that of the surrounding reservoir rocks, consequently lowering the average temperature of the production well.

The determination of the well spacing for production and reinjection and the distribution of the well pattern depend on the geological structure and seepage law of the thermal reservoir. The optimal well spacing can delay the propagation time of the cold front surface, reduce fluid loss, and ensure that the thermal reservoir pressure is compensated. Fig. 13c shows the influence of changing the distance between production and reinjection wells on the average temperature of the production wells under the same reinjection flow rate (60 m^3/h) and temperature (25°C) conditions. When the distances between the extraction and reinjection wells were 340 m, 440 m, and 540 m respectively, the average temperatures of the extraction Wells after the geothermal system had been in operation for 100 a were 152°C, 163.7°C, and 168.1°C, respectively. The increase in the spacing between production and reinjection wells lead to an increase in the seepage path of reinjection water. Reinjection water has more time and space to absorb the heat from the thermal reservoir, enhancing the heat transfer effect, and thus the average temperature drop rate and decrease of the extraction well gradually decrease.

4.5 Thermal breakthrough prediction analysis

According to DZ/T 0331–2020 "Evaluation Methods and Estimation Regulations for Geothermal Resources", the thermal breakthrough time of geothermal wells can be calculated based on a 2°C drop in the temperature of the geothermal reservoir after 100 a of exploitation under reinjection conditions. Therefore, this study stipulates that the thermal breakthrough time of the mining well is the time when the temperature of the mining well drops by 2°C after 100 a of operation of the geothermal system's production and injection. That is, a thermal breakthrough occurs when the temperature of the mining well drops to 167°C. The temperature change in the production well over 100 a, predicted by the numerical model, is shown in Fig. 14. The results show that around the 78th year, the temperature of the production well dropped to 167°C, and a thermal breakthrough occurred.

4.6 Optimization strategies and uncertainty analysis

Fig. 14 suggests a differential influence among reinjection temperature, flow rate, and production-reinjection well spacing on production well temperature. While alterations in reinjection flow rate and well spacing exert a considerable impact on seepage heat transfer within the thermal reservoir, variations in reinjection temperature appear to have a comparatively lesser effect. In practical engineering applications, careful consideration should be given to optimizing both the production-injection flow rates and well spacing. Furthermore, a cascading utilization of extracted geothermal water prior to reinjection is recommended. The formulation of an optimized reinjection strategy is crucial for enhancing heat extraction efficiency and prolonging the operational lifespan of the geothermal well system. Model predictions indicate that elevating the reinjection temperature, reducing the flow rate, and expanding well spacing contribute to varying degrees of extension in the geothermal reservoir's development life. Based on the temperature changes of the extraction well after the geothermal system has been in operation for 100 a as obtained from 27 numerical simulation results (Table 7), it is concluded that with the decreasing well spacing, the influence of reinjection temperature and reinjection flow rate on the temperature of the production well gradually becomes significant.

In addition, the critical well spacing for thermal breakthrough under two working conditions was studied: One with a reinjection flow rate of 60 m^3/h and a reinjection temperature of 80°C, and the other with a reinjection flow rate of 60 m^3/h and a reinjection temperature of 25°C. The simulation results show that when the reinjection flow rate is 60 m^3/h, the reinjection temperature is 80°C, and the well spacing is at least 470 m, it can meet the requirement of no thermal breakthrough. When the reinjection flow rate is 60 m^3/h, the reinjection temperature is 25°C, and the well spacing is at least 510 m, it can ensure that no thermal breakthrough occurs. Based on on-site tests, the reinjection scheme and well location layout were optimized. It was concluded that when the reinjection flow rate is 60 m^3/h, the reinjection temperature is 80°C, and the well spacing is at least 470 m, the temperature change of the mining well does not

Table 7 Temperature variation and thermal breakthrough time of the mining well after 100 a of the geothermal system operation under different reinjection schemes

Well spacing	Reinjection flow	Reinjection temperature		
		25°C	50°C	80°C
340 m	60 m^3/h	152°C/38a	154°C/41a	157°C/46a
	100 m^3/h	143.9°C/28a	146.3°C/29a	150.7°C/33a
	140 m^3/h	135.8°C/23a	139.6°C/24a	145.49°C/30a
440 m	60 m^3/h	163.7°C/70a	164.5°C/74a	165.6°C/78a
	100 m^3/h	159.9°C/54a	161.3°C/58a	163°C/65a
	140 m^3/h	155.8°C/46a	157.8°C/49a	160.2°C/55a
540 m	60 m^3/h	168.1°C/No thermal breakthrough	168.3°C/No thermal breakthrough	168.5°C/No thermal breakthrough
	100 m^3/h	167.2°C/No thermal breakthrough	167.5°C/No thermal breakthrough	167.9°C/No thermal breakthrough
	140 m^3/h	166.2°C/90a	166.7°C/96a	167.2°C/No thermal breakthrough

Notes: "165.6°C/78a" represents the temperature value of the extraction well after the geothermal system has been in operation for 100 a, the time of thermal breakthrough under the current reinjection scheme.

exceed 2°C after the geothermal system operates for 100 a, and no thermal breakthrough will be triggered.

However, the applicability of this optimization strategy is limited to the specific geothermal extraction and reinjection system of the on-site test due to the inherent variability of geological conditions. Moreover, the fracture network, particularly faults, serves as the primary conduit for fluid movement and heat transfer in metamorphic rock geothermal reservoirs. This influences not only the seepage heat transfer process of geothermal fluids but also the evolution of the temperature field within the reservoir. Due to the fact that the tracer sodium naphthalene sulfonate used in the tracer test is a conservative tracer with certain limitations, it can only determine that there are a few seepage channels in the thermal reservoir connecting the production well and the reinjection well, and cannot accurately identify the morphology and distribution of the fracture network in the metamorphic rock thermal reservoir. Therefore, in the simulation study, a fracture channel was assumed to be equivalent to the fracture network connected between injection wells, without considering the heterogeneity of the fracture network in the thermal reservoir. In future research, the spatial heterogeneity of the fracture network of metamorphic rock thermal reservoirs will be considered in combination with field test data to deeply study the seepage heat transfer mechanism of metamorphic rock thermal reservoirs.

5 Conclusions

This study takes the high-temperature metamorphic rock thermal reservoir in the Tianzhen geothermal field of Datong City as the object. Through conducting reinjection tracer tests and establishing a seepage heat transfer model of the thermal reservoir, the seepage laws and seepage heat transfer processes of the high-temperature metamorphic rock thermal reservoir during the reinjection process are revealed. The distribution characteristics of various physical fields in the geothermal reservoir after the geothermal system has been in operation for 100 a were also predicted. The influence of different reinjection schemes on seepage heat transfer in the geothermal reservoir was analyzed, and the optimization strategy of the reinjection scheme was proposed. The conclusions are as follows:

(1) The tracer recovery rate is relatively low, indicating poor connectivity between production and injection wells. Within the geothermal reservoir, only a limited number of seepage channels are present to establish connectivity between production wells and reinjection wells. In these seepage channels, the average flow velocity of the reinjected fluid is measured at 11.6 m/d. Additionally, a portion of the fluid migrates toward the shallow layers along water-conducting fractures.

(2) Driven by pressure differences, the reinjected fluid flows toward production wells or around the geothermal reservoir in different directions, with only a small portion flowing toward production wells through connected seepage channels. In the initial stage of reinjection, a low-temperature zone and a cold front are formed around the injection well, and the morphology of the cold front is affected by the fractured seepage channels. As reinjection continues, the cold front continuously migrates and expands until it reaches the production well, causing temperature changes in the production well.

(3) The changes in the reinjection flow rate and the well spacing for production and injection have a significant impact on the seepage heat transfer of the thermal reservoir, while the decrease in the reinjection temperature has a relatively small influence on the seepage heat transfer of the thermal reservoir. The lower the reinjection temperature, the greater the flow rate, the smaller the well spacing, and the greater the rate and extent of temperature drop in the mining well.

(4) Under the current reinjection test conditions, the temperature of the production well in the geothermal system has dropped by 4°C after 100 a of operation, and a thermal breakthrough occurred at 78 a. To extend the development life of geothermal reservoirs, while maintaining a reinjection flow rate of 60 m^3/h and a reinjection temperature of 80°C unchanged, the well spacing should be no less than 470 m to ensure that the temperature change of the extraction well is less than 2°C after 100 a of reinjection operation, and no thermal breakthrough will be triggered.

Acknowledgements

This research was supported by the National Natural Science Foundation of China (No.42272350), Shanxi Key Laboratory for Exploration and Exploitation of Geothermal Resources (Grant Nos. SX202601).

References

Al-Khoury R, Bonnier PG, Brinkgreve RBJ. 2005. Efficient finite element formulation for

geothermal heating systems. Part I: Steady state. International Journal for Numerical Methods in Engineering, 63(7): 988−1013. DOI：10.1002/nme.1313.

Al Khoury R, Bonnier P. 2006. Efficient finite element formulation for geothermal heating systems. Part II: transient. International journal for numerical methods in engineering, 67(5): 725−745. DOI：10.1002/nme.1662.

Allen A, Milenic D. 2003. Low-enthalpy geothermal energy resources from groundwater in fluvioglacial gravels of buried valleys. Applied Energy, 74(1): 9−19. DOI：10.1016/S0306-2619(02)00126-5.

Aquilina L, de Dreuzy JR, Bour O, et al. 2004. Porosity and fluid velocities in the upper continental crust (2 to 4 km) inferred from injection tests at the Soultz-sous-Forêts geothermal site. Geochimica et Cosmochimica Acta, 68(11): 2405−2415. DOI：10.1016/j.gca.2003.08.023.

Axelsson G, Björnsson G, Montalvo F. 2005. Quantitative interpretation of tracer test data. Proceedings World Geothermal Congress Antalya, Turkey: 24−29.

Cao Q, Fang CH, Li Y, et al. 2021. Development status and enlightenment of geothermal reinjection at home and abroad. Oil Drilling and Production Technology, 43(02): 203−211. DOI：10.13639/j.odpt.2021.02.011.

Cen M, Dong S, Shi W, et al. 2015. Structural analysis on the formation mechanism of Datong Basin. Geological Review, 61(6): 1235−1247. DOI：10.16509/j.georeview.2015.06.004.

Cui YL, Zhu J, Twaha S, et al. 2018. A comprehensive review on 2D and 3D models of vertical ground heat exchangers. Renewable and Sustainable Energy Reviews, 94: 84−114. DOI：10.1016/j.rser.2018.05.063.

Diaz AR, Kaya E, Zarrouk SJ. 2016. Reinjection in geothermal fields−A worldwide review update. Renewable and Sustainable Energy Reviews, 53: 105−162. DOI：10.1016/j.rser.2015.07.151.

Du L, Zhao L, Qiao Y, et al. 2019. Study on the influence of fracture orientation and injection velocity on the micro seepage law of reinjection water in fracture geothermal reservoir. Shandong Chemical Industry, 48(20): 139−141,146. (in Chinese) DOI：10.19319/j.cnki.issn.1008-021x.2019.20.052.

Fan Y, Duan Z, Yang Y, et al. 2023. Impact of reservoir characteristics on the well spacing of sandstone geothermal reservoir: A case study of Jiyang Depression. Hydrogeology and Engineering Geology, 51(1): 215−223. DOI：10.16030/j.cnki.issn.1000-3665.202301033.

Hawkins AJ, Fox DB, Becker MW, et al. 2017. Measurement and simulation of heat exchange in fractured bedrock using inert and thermally degrading tracers. Water Resources Research, 53(2): 1210−1230. DOI：10.1002/2016WR019617.

He Y, Jia X, Zhang Z, et al. 2023. A study of the formation mechanism and resource developmentprospect of the high-temperature geothermal systemin the Yanggao-Tianzhen area. Hydrogeology and Engineering Geology, 50(4): 39−49. (in Chinese) DOI：10.16030/j.cnki.issn.1000-3665.202302065.

He YY, Bai B, Hu SB, et al. 2016. Effects of surface roughness on the heat transfer characteristics of water flow through a single granite fracture. Computers and Geotechnics, 80: 312−321. DOI：10.1016/j.compgeo.2016.09.002.

Huang Y, Zhang Y, Yu Z, et al. 2019. Experimental investigation of seepage and heat transfer in rough fractures for enhanced geothermal systems. Renewable Energy, 135: 846−855. DOI：10.1016/j.renene.2018.12.063.

Huang YB, Zhang YJ, Gao XF, et al. 2021. Experimental and numerical investigation of seepage and heat transfer in rough single fracture for thermal reservoir. Geothermics, 95: 102163. DOI：10.1016/j.geothermics.2021.102163.

Juliusson E, Horne RN. 2013. Characterization of fractured reservoirs using tracer and flow-rate data. Water Resources Research, 49(5): 2327−2342. DOI：10.1002/wrcr.20220.

Kamila Z, Kaya E, Zarrouk SJ. 2021. Reinjection in geothermal fields: An updated worldwide review 2020. Geothermics, 89: 1−88. DOI：10.1016/j.geothermics.2020.101970.

Kuo CH, Song SR, Rose P, et al. 2018. Reactive tracer experiments in a low temperature geothermal field, Yilan, Taiwan. Geothermics, 74: 298−304. DOI：10.1016/j.geother-

mics.2017.11.017.

Kusky TM, Li J. 2003. Paleoproterozoic tectonic evolution of the North China Craton. Journal of Asian Earth Sciences, 22(4): 383−397. DOI：10.1016/S1367-9120(03)00071-3.

Li TX, Cai YF, Liu YG, et al. 2020. Tracer test and simulation of thermal energy storage in carbonate rocks of the Xian County geothermal field. Earth Science Frontiers, 27(01): 152−158. DOI：10.13745/j.esf.2020.1.16.

Liu GH, Pu H, Zhao ZH, et al. 2019a. Coupled thermo-hydro-mechanical modeling on well pairs in heterogeneous porous geothermal reservoirs. Energy, 171: 631−653. DOI：10.1016/j.energy.2019.01.022.

Liu HJ, Wang HW, Lei HW, et al. 2020. Numerical modeling of thermal breakthrough induced by geothermal production in fractured granite. Journal of Rock Mechanics and Geotechnical Engineering, 12(4): 900−916. DOI：10.1016/j.jrmge.2020.01.002.

Liu JR. 2003. The status of geothermal reinjection. Hydrogeology and Engineering Geology, 30(3): 100−104. (in Chinese)

Liu M, Cui X, Liu F. 2004. Cenozoic rifting and volcanism in eastern China: A mantle dynamic link to the Indoa-Asian collision? Tectonophysics, 393(1-4): 29−42. DOI：10.1016/j.tecto.2004.07.029.

Liu YG, Liu GH, Zhao ZH, et al. 2019b. Theoretical model of geothermal tail water reinjection based on an equivalent flow channel model: A case study in Xianxian, North China Plain. Energy Exploration and Exploitation, 37(2): 849−864. DOI：10.1177/0144598718822401.

Liu YG, Long XT, Liu F. 2022. Tracer test and design optimization of doublet system of carbonate geothermal reservoirs. Geothermics, 105: 102533. DOI：10.1016/j.geothermics.2022.102533.

Ma YQ, Zhang YJ, Hu ZJ, et al. 2019a. Experimental study of the heat transfer by water in rough fractures and the effect of fracture surface roughness on the heat transfer characteristics. Geothermics, 81: 235−242. DOI：10.1016/j.geothermics.2019.05.009.

Ma YQ, Zhang YJ, Huang YB, et al. 2019b. Experimental study on flow and heat transfer characteristics of water flowing through a rock fracture induced by hydraulic fracturing for an enhanced geothermal system. Applied Thermal Engineering, 154: 433−441. DOI：10.1016/j.applthermaleng.2019.03.114.

O'Sullivan MJ, Pruess K, Lippmann MJ. 2001. State of the art of geothermal reservoirs simulation. Geothermics, 30(4): 395−429. DOI：10.1016/S0375-6505(01)00005-0.

Pan L, Meng L, Sun F, et al. 2023. Geothermal geological characteristics and resourcepotential in the north of Datong Basin, Shanxi Province. Geology in China, 50(6): 1632−1645. (in Chinese) DOI：10.12029/gc20220304001.

Pandey SN, Vishal V, Chaudhuri A. 2018. Geothermal reservoir modeling in a coupled thermo-hydro-mechanical-chemical approach: A review. Earth-Science Reviews, 185: 1157−1169. DOI：10.1016/j.earscirev.2018.09.004.

Qiao Y, Li S, Yan K, et al. 2023. Karst thermal reservoir tracer test and seepage characteristics analysis in Niutuozhen geothermal field in Xiongan New Area. Frontiers in Earth Science, 11: 01−09. DOI：10.3389/feart.2023.1132095.

Radilla G, Sausse J, Sanjuan B, et al. 2012. Interpreting tracer tests in the Enhanced Geothermal System (EGS) of Soultz-sous-Forêts using the equivalent stratified medium approach. Geothermics, 44: 43−51. DOI：10.1016/j.geothermics.2012.07.001.

Ren YQ, Kong YL, Pang ZH, et al. 2023. A comprehensive review of tracer tests in enhanced geothermal systems. Renewable and Sustainable Energy Reviews, 182: 113393. DOI：10.1016/j.rser.2023.113393.

Rose PE, Benoit WR, Kilbourn PM. 2001. The application of the polyaromatic sulfonates as tracers in geothermal reservoirs. Geothermics, 30(6): 617−640. DOI：10.1016/S0375-6505(01)00024-4.

Sanford WE, Cook PG, Robinson NI, et al. 2006. Tracer mass recovery in fractured aquifers estimated from multiple well tests. Groundwater, 44(4): 564−573. DOI：10.1111/j.1745-6584.2006.00161.x.

Stefansson V. 1997. Geothermal reinjection experience. Geothermics, 26(1): 99−139. DOI：10.1016/S0375-6505(96)00035-1.

Tang JP, Qiu YM. 2023. Analysis of the influence

of the distance between producing Wells on the enhancedgeothermal system. Chinese Journal of Computational Mechanics, 40(01): 126−132. DOI: jslxxb.cn/index.php/jslxxb/article/view/4256.

Wang GL, Liu YG, Zhu X, et al. 2020a. The status and development trend of geothermal resources in China. Earth Science Frontiers, 27(01): 1−9. DOI：10.13745/j.esf.2020.1.1.

Wang GL, Lu C. 2023. Stimulation technology development of hot dry rock and Enhanced geothermal system driven by carbon neutrality target. Geology and Resources, 32(01): 85−95. DOI: 10.13686/j.cnki.dzyzy.2023.01.011.

Wang GS, Song XZ, Shi Y, et al. 2020b. Comparison of production characteristics of various coaxial closed-loop geothermal systems. Energy Conversion and Management, 225: 113437. DOI：10.1016/j.enconman.2020.113437.

Wang B, Okiambe E, Omenda P, et al. 2014. A numerical solution to estimate hydro-geologic parameters of a fractured geothermal porous medium based on fluorescein thermal decay correction. Geothermics, 51: 124−129. DOI：10.1016/j.geothermics.2013.11.003.

Wang Y, Liu Y, Bian K, et al. 2021. Influence of low temperature tail water reinjection on seepage and heat transfer of carbonate reservoirs. Energy Exploration ang Exploitation, 39(6): 2062−2079. DOI：10.1177/01445987211020416.

Yao J, Zhang X, Huang Z, et al. 2022. Numerical simulation of thermo–hydraulic coupling processes in fractured karst geothermal reservoirs. Natural Gas Industry, 9(6): 511−520. DOI：10.1016/j.ngib.2022.11.003.

Yu C, Zhang Y, Tan Y, et al. 2023. Simulation study of novel methods for water reinjection efficiency improvement of a doublet system in guantao sandstone geothermal reservoir. Geothermics, 111: 102709. DOI：10.1016/j.geothermics.2023.102709.

Zhang P, Zhang Y, Huang Y. 2021. Experimental study of convective heat transfer characteristics of fractures with different morphologies based on fractal theory. Case Studies in Thermal Engineering, 28: 101499. DOI：10.1016/j.csite.2021.101499.

Zhao Z, Dou Z, Liu G, et al. 2021. Equivalent flow channel model for doublets in heterogeneous porous geothermal reservoirs. Renewable Energy, 172: 100−111. DOI：10.1016/j.renene.2021.03.024.

Zheng J, Li P, Dou B, et al. 2022. Impact research of well layout schemes and fracture parameters on heat production performance of enhanced geothermal system considering water cooling effect. Energy, 255: 124496. DOI：10.1016/j.energy.2022.124496.

Zhou LM, Zhu ZD, Xie XH, et al. 2022. Coupled thermal–hydraulic–mechanical model for an enhanced geothermal system and numerical analysis of its heat mining performance. Renewable Energy, 181: 1440−1458. DOI：10.1016/j.renene.2021.10.014.

Zhou W, Hu X, Yan S, et al. 2020. Genetic analysis of geothermal resources and geothermal geological characteristics in Datong basin, Northern China. Energies, 13(7): 1792. DOI：10.3390/en13071792.

Zhu R, Xu Y, Zhu G, et al. 2012. Destruction of the North China craton. Science China Earth Sciences, 55: 1565−1587. DOI：10.1007/s11430-012-4516-y.

Zinsalo JM, Lamarche L, Raymond J. 2020. Injection strategies in an enhanced geothermal system based on discrete fractures model. Applied Thermal Engineering, 169: 114812. DOI：10.1016/j.applthermaleng.2019.114812.